Postharvest Biology and Technology 153 (2019) 161–168

Contents lists available at ScienceDirect

Postharvest Biology and Technology

journal homepage: www.elsevier.com/locate/postharvbio

Validation study for measuring absorption and reduced scattering coefficients by means of laser-induced backscattering imaging

Manuela Zude-Sasse[a,*], Norhashila Hashim[a,b], Roland Hass[c], Nabarun Polley[c], Christian Regen[a]

[a] Department of Horticultural Engineering, Leibniz Institute for Agricultural Engineering and Bioeconomy (ATB), 14469 Potsdam-Bornim, Germany
[b] Department of Biological and Agricultural Engineering, Faculty of Engineering, Universiti Putra Malaysia, Malaysia
[c] Physical Chemistry – InnoFSPEC, Institute of Chemistry, University of Potsdam, 14476 Potsdam-Golm, Germany

ARTICLE INFO

Keywords:
Absorption
European pear
Fruit quality
Phantoms
Reduced scattering coefficient
Scattering
Spatially resolved spectroscopy

ABSTRACT

Decoupling of optical properties appears challenging, but vital to get better insight of the relationship between light and fruit attributes. In this study, nine solid phantoms capturing the ranges of absorption (μ_a) and reduced scattering (μ_s') coefficients in fruit were analysed non-destructively using laser-induced backscattering imaging (LLBI) at 1060 nm. Data analysis of LLBI was carried out on the diffuse reflectance, attenuation profile obtained by means of Farrell's diffusion theory either calculating μ_a [cm^{-1}] and μ_s' [cm^{-1}] in one fitting step or fitting only one optical variable and providing the other one from a destructive analysis. The nondestructive approach was approved when calculating one unknown coefficient non-destructively, while no ability of the method was found to analysis both, μ_a and μ_s', non-destructively. Setting μ_s' according to destructive photon density wave (PDW) spectroscopy and fitting μ_a resulted in root mean square error (rmse) of 18.7% in comparison to fitting μ_s' resulting in rmse of 2.6%, pointing to decreased measuring uncertainty, when the highly variable μ_a was known.

The approach was tested on European pear, utilizing destructive PDW spectroscopy for setting one variable, while LLBI was applied for calculating the remaining coefficient. Results indicated that the optical properties of pear obtained from PDW spectroscopy as well as LLBI changed concurrently in correspondence to water content mainly. A destructive batch-wise analysis of μ_s' and online analysis of μ_a may be considered in future developments for improved fruit sorting results, when considering fruit with high variability of μ_s'.

1. Introduction

Developments in non-destructive optical techniques were studied by many working groups world-wide and commercialized for the analysis of fresh produce quality. The optical analysis has been widely explored for in-situ sensing, sorting, and grading fresh produce. As light hits tissue, the propagated light is absorbed, transmitted or reflected forward and reflected backward (diffusely reflected) near to the incident point (Birth, 1976; Chen, 1978). Using frequency-, time-, and spatially resolved techniques, the sum signal of absorption and scattering is measured. In the analyses of fruit and vegetables, numerous studies using frequency-based spectroscopy in the visible and shortwave near infrared wavelength range (vis/SWNIR), plotting the measured light intensity over the wavelength, have been conducted to evaluate the changes of fruit quality parameters such as firmness, soluble solids content (SSC), dry matter, internal disorders, and pH (Nicolaï et al., 2008; Cao et al., 2010; Mendoza et al., 2014; Sun et al., 2016). However, it became obvious that frequency-based diffuse reflectance readings always need recalibration due to changes in both, the absorption and the scattering (Cubeddu et al., 2001; Zude et al., 2011; Seifert et al., 2015). Consequently, the separated analysis of μ_a and μ_s' was targeted.

The spatially resolved approach gained interest, since the analysis elegantly deals with the problem and the measuring set-up can be achieved with easily accessible, commercial modules considering light source and detector. The radial profile over the distance between incident point and measuring point of propagated light that is diffusely reflected, carries potentially useful information of tissue's attributes. Statistical models and equations discussing the shape and integral of the radial profile have been developed to determine expressions for the dependence of the diffuse reflectance in radial distance from the light source. The models such as derivation of Green's function (Groenhuis et al., 1983a, b) and extended study of its application were carried out by Steinke and Shepherd (1986) and Schmitt et al. (1990) predicting the changes in diffuse reflectance at a single radial position from blood in a cuvette as the haemoglobin oxygenation varied. The expression for

* Corresponding author.
E-mail address: mzude@atb-potsdam.de (M. Zude-Sasse).

https://doi.org/10.1016/j.postharvbio.2019.04.002
Received 8 September 2018; Received in revised form 20 March 2019; Accepted 3 April 2019
Available online 16 April 2019

the radial reflectance, however, is not a closed form function of the radial distance and the optical properties, and so does not easily permit analysis of the optical properties. With the assumption that scattering is isotropic, Farrell and Patterson (1992) vindicated absorption coefficient (μ_a) and reduced scattering coefficient (μ_s') as quantitative fundamental parameters for the interaction between light and tissue. Since most biological materials including food are scattering dominant, Farrell's model was assumed eligible describing the optical properties of perishables.

The spatially resolved approach was introduced for the non-destructive analysis of fruit and vegetables by Lu and co-workers (Qin and Lu, 2008) providing a new data source on the fresh produce. Absorption and reduced scattering spectra of several fruit and vegetables were obtained non-destructively by means of hyperspectral backscattering imaging (Qin and Lu, 2008). The radial profiles were extracted over 500–1000 nm from the acquired, pre-processed images, followed by the procedure of fruit size corrections for the spatial profiles due to the light intensity distortion caused by the curved fruit surface. Then, the Farrell diffusion theory model was used to fit the corrected experimental data using a trust-region nonlinear least squares fitting algorithm. The absorption spectrum in the visible wavelength range revealed the major groups of pigments, i.e., chlorophyll, anthocyanin, and carotenoids, while in the near infrared wavelength range overtones are measured of the absorption of C–H, C−OH, and −OH in the fruit and vegetables samples. The reduced scattering spectrum decreases towards the longer wavelengths with different values and slopes for different commodities and are reported as being influenced by the particle size of scatters (Seifert et al., 2015). This may potentially relate to the mechanical properties of fruit and vegetables.

Correlation analysis of the optical properties and fruit, particularly pear attributes, showed various results: Nicolaï et al. (2008) observed a nonlinear relationship between reduced scattering coefficient obtained by means of time resolved analysis at 900 nm and firmness of 'Conference' pear measured using Magness Taylor test. Mendoza et al. (2014), in their attempt to grade apples using frequency-based vis/SWNIR spectroscopy and spatially resolved approach in similar wavelength range found that frequency-based spectroscopy provide better sorting results with percentage of correct classification ranging between 87% and 98% for firmness while 77% and 92% for SSC, respectively. Similar results were found when measuring apple firmness using multispectral scattering imaging and spatially resolved reflectance spectroscopy (Sun et al., 2016). Sun et al. (2016) even found that variables taken from Lorentzian model outperformed diffusion theory. Similar results were found by Lorente et al. (2015), who used laser light at few wavelengths for the spatially resolved readings of backscattered images (LLBI). This is surprising, since the scattering method analysed by means of diffusion theory should provide more detailed information on the potentially separated μ_a and μ_s', compared to the sum signal obtained from purely frequency-resolved vis/SWNIR spectroscopy. The reason for such findings may be the limit of fitting capability of the Farrell diffusion theory in spatially resolved method for segregating the optical properties. Furthermore, the use of optical properties to analyse the quality of fruit relies on statistical methods to relate spectral features to the fruit property, which may lead to overfitting, using variances in the optically obtained data set which are only indirectly related to the fruit property under question.

To obtain reliable data on the optical properties of the fruit, reference measurements on thin slices of the fruit tissue can be carried out by means of integrating spheres set-up using adding-doubling (IAD) method for measuring the ballistic, diffuse transmitted, scattered, and absorbed photons separately (Prahl et al., 1993). Rowe et al. (2014) used the destructive method by applying single integrating sphere technique to measure the μ_a and μ_s' of apples from 400 to 1050 nm and identified reliable relationships with coefficient of determination $R^2 > 0.4$ between Magness Taylor fruit flesh firmness, acoustic stiffness and the optical properties. He et al. (2016) assessed firmness and SSC of pear based on μ_a and μ_s' using an automatic integrating sphere system from 400 to 1150 nm. To quantify the estimation errors of the μ_a and μ_s', the system was verified by using a set of commercial solid phantoms and a set of liquid phantoms. Results indicated encouraging results with average errors of estimation of μ_a and μ_s' at 4.9% and 3.5%, respectively, and the R^2 values being approx. 0.4 and 0.5 for the relationships between optical properties and SSC and firmness, respectively.

Alternative methods are presently explored (Adebayo et al., 2017; Lu and Lu, 2018). As one alternative, the photon density wave (PDW) spectroscopy (Bressel et al., 2013) uses intensity-modulated laser light that is guided into the sample with an optical fiber. The fiber end acts as a point light source. Further receiving fibers are placed in different distance to the emission fiber. Due to the immersion of the optical fibers into the sample, PDW spectroscopy can be referred to as destructive method with respect to fruit analysis. Further application examples of PDW spectroscopy include biotechnological processes (Hass et al., 2015), and food monitoring (Vargas Ruiz et al., 2012.). Due to the interaction of the intensity modulated light with the material by absorption and multiple scattering, a PDW is created. The shift of the amplitude and the phase of the PDW are characterized as function of emitter/detector-fiber distance and modulation frequency. As a result, the absorption and reduced scattering coefficient are obtained independently and at an experimental error lower than 1% (Reich et al., 2003). In this work, the values obtained from PDW spectroscopy are expressed as μ_a* and μ_s'* to differentiate from the results obtained by LLBI. Recently, a study of LLBI coupled with PDW spectroscopy as reference method to determine μ_a and μ_s' was conducted for non-destructive analyses of flesh firmness and SSC in pear (Adebayo et al., 2017). By using Farrell diffusion theory model, the results indicated $R^2 = 0.4$ for calibration model using μ_a to predict SSC at 532 nm and 830 nm, and $R^2 = 0.8$ for μ_s' to predict firmness at 660 and 830 nm. Although promising results were obtained for measuring firmness and SSC, the consistency of the experimental design is still intangible. Thus, an extension study was suggested to improve and validate the recent works. Hence, in this study, validation analysis was carried out using solid-state phantoms providing the range of μ_a and μ_s' that can be expected in pear. The specific objectives of this study were (i) to validate the approach of non-destructive LLBI combined with reference data on solid-state phantoms with known optical properties, and (ii) to determine the μ_a and μ_s' of pear by LLBI using reference data of either μ_a* or μ_s'* obtained by means of PDW spectroscopy.

2. Materials and methods

2.1. Samples

A set of commercial solid-state phantoms (PDW Analytics GmbH, Potsdam, Germany) was analysed, which consists of nine resin moulding compounds, shaped as cylinders with a half-sphere end on one side with cylinder and sphere radius of 5 cm. The 9 phantoms have individually mixed absorber and scatterer fractions, so that the optical coefficients of the phantoms varied from 0.103 to 1.265 cm^{-1} for μ_a* and 2.020 to 22.100 cm^{-1} for μ_s'* (Table 1, cf. Fig. 3).

The actual optical properties were obtained by PDW spectroscopy from the liquid resin matrix including absorber and scatterer. Comparison studies between liquid and subsequently solidified solid-state phantom by drilling holes for the optical fibers into the phantoms indicated general agreement of the optical properties. However, the positional errors for the fiber ends induced by drilling long, thin holes for the fibers caused high measuring uncertainty. Thus, the values for the liquid resin matrix are used here.

Data acquisition on pears was conducted on good quality, commercially graded pears (*Pyrus communis* L. 'Packham's Triumph'). The data collection took place after CA storage, in shelf life over a period of 17 days involving four sampling days: Day 1 on 3rd April 2017; Day 4 on 6th April 2017; Day 8 on 10th April 2017; Day 17 on 19th April 2017.

Table 1
Absorption coefficient and reduced scattering coefficients [cm^{-1}] with standard error of three measurements of solid-state phantoms measured at wavelength 940 nm.

Phantom	Absorption coefficient, μ_a*	Reduced scattering coefficient, μ_s'*
A.1	0.1084 ± 0.0006	2.087 ± 0.009
A.2	0.5440 ± 0.0150	2.110 ± 0.065
A.3	1.2100 ± 0.2800	2.020 ± 0.640
B.1	0.1033 ± 0.0002	11.680 ± 0.020
B.2	0.4494 ± 0.0056	11.880 ± 0.150
B.3	1.2080 ± 0.0370	11.680 ± 0.380
C.1	0.1059 ± 0.0002	22.100 ± 0.024
C.2	0.4766 ± 0.0032	21.590 ± 0.150
C.3	1.2650 ± 0.0460	20.800 ± 0.790

The samples were stored at 15 °C, which was maintained during all measurements ± 2 °C. In total, 80 pears were measured for this study by which 20 pears were measured for each sampling day.

The measurement started with the application of LLBI followed by PDW spectroscopy and analytical methods for measuring firmness, SSC and water content. Analytical methods were conducted subsequently measurements of LLBI and PDW spectroscopy. The firmness of the samples was measured by using texture analyser (XT plus, Stable Micro System, UK) with 11.13 mm cylindrical probe at a velocity of 200 mm min^{-1}. The maximum force as the probe penetrated the fruit flesh was corrected by the probe diameter and taken as a firmness value of the fruit, expressed as N cm^{-2}. The SSC values in % were measured with digital refractometer (DR 301-95, A. Krüss Optronic, Germany) by placing a drop of the pear juice onto the glass plate. The measurement was repeated (n = 3) and the average values were recorded. Measurement of water content was conducted gravimetrically before and after oven-drying at 85 °C for 48 h. The water content was calculated by expressing the mass difference as percentage of mass before drying.

2.2. Acquisition of backscattering images

The backscattering images of pears were acquired using LLBI system that was developed and assembled by the Leibniz Institute for Agricultural Engineering and Bioeconomy (ATB) Germany (Qing et al., 2008). The system comprised of a laser diode (LPM-1060-85E, Newport, USA) emitting at 1060 nm and directed towards the fruit surface at 15° incident angle, monochrome charge coupled device (CCD) camera (CV- A50IR, JAI Ltd, Japan) located vertically at the centre of the system, with a F2.5 zoom lens and 18–108 mm focal length (12VG1040 ASIR-SQ, Tamron Co. Ltd, Japan) and a computer to control laser diodes and the camera (Baranyai and Zude, 2009). The system has been facilitated with an auto-adjusted moving platform to assist the setting of the height and control the distance and angle between sample and CCD camera. The acquired images were processed using in-house developed, automated image processing protocol (Labview version 6.1, National Instruments, USA).

Images were taken in the dark. One image was acquired for each sample with the size 720 × 576 pixel, resulting in total of 89 images for all samples. The geometric calibration of the system was 0.1205 mm per pixel. The measurement of phantoms and pears using LLBI provide the attenuation profile of light intensity per pixel value in radial direction. Analysis of μ_a and μ_s' was conducted by means of Farrell's algorithm (i) to fit both optical properties, μ_a and μ_s', to the radial profile and (ii) using the same protocol as described by Adebayo et al. (2017). In the latter approach, the absolute values of either μ_a* or μ_s'* obtained from PDW spectroscopy was applied to calculate the remaining variable, μ_s' or μ_a, respectively. The fitting process was carried out using Marquardt-Leavenworth routine by reducing the root mean square error (rmse) in 10,000 iterations.

2.3. PDW spectroscopy

A PDW spectrophotometer (PDW Analytics GmbH, Potsdam, Germany) was applied to measure fruit as well as phantoms at the Applied Analytical Photonics Laboratory, University of Potsdam, Germany. The system was own-developed with main components being a vector network analyzer (ZVA8, Rohde & Schwarz GmbH & Co. KG, Munich, Germany) as analytic tool, laser diodes with controller, amplifier and computer for spectrometer control and data analysis (Bressel et al., 2013; Hass et al., 2015). The vector network analyzer generates a sinusoidal electrical high-frequency signal with modulation range covering 10–1300 MHz to generate the high-frequency modulated laser current together with a BIAS-T.

Phantoms were measured at 940 nm as described above, while fruit measurement was conducted at 940 nm by inserting the in-house developed and manufactured probe into the middle of a pear. The probe was designed to reduce fiber positioning error that allow for spatial multiplexing automatically with the help of a fiber-optical switch. The probe consists of multiple optical fibres with 600 µm core diameter (JTFLH600, Laser Components GmbH, Germany) stabilized in metal cannula designated at a distance of 4.88, 8.03, 11.11, 14.07, 17.01, 20.04, 23.11 and 25.88 mm from the emission fiber. The intensity modulated light from the laser diode (Thorlabs GmbH, Munich, Germany) was guided into the sample through the emission fiber. The emission fiber works as a point light source while the other optical fibers guided the light out of the sample to the light detector, an avalanche photon diode (APM-400 P, Becker & Hickl GmbH, Berlin, Germany). The resulting signal was then analyzed by the vector network analyzer with respect to the changes in phase and amplitude. The absolute values of μ_a* and μ_s'* of the samples were extracted based on the earlier methodological works as described in detail by Bressel et al. (2013) and Hass et al. (2015).

2.4. Analysis and validation of μ_a and μ_s'

Statistical analysis was carried out subsequently to test differences between calculated and reference values of the phantoms using the root mean square error (rmse) to describe the percentage discrepancy between reference and calculated μ_a and μ_s' values. Statistical analysis was conducted using Matlab (R2013a) to carry out a two-way analysis of variance (ANOVA) and Tukey's test at $P \leq 0.05$ significant level, while linear regression was adopted for predicting pear quality.

3. Results and discussion

3.1. Validation of experimental set-up using solid-state phantoms

Each phantom is characterised at 940 nm representing μ_a* and μ_s'* values (Table 1) according to the ranges expected in fresh fruit. Phantom A.1 has the lowest values of μ_a* and μ_s'* and hence, shows the largest backscattered spot size in the image measured using LLBI at 1060 nm (Fig. 1). In contrast, phantom C.3 has the highest value of μ_a* and μ_s'*, which resulted in the smallest spot size in LLBI. However, the spot sizes in the intermediate range appear visually difficult to distinguish.

From each LLBI image, the radial profile was obtained as the intensity measured over the distance from incident point until 20 mm, when the light was attenuated in all samples. These mean attenuation profiles of the phantoms were calculated by means of Farrell's diffusion theory using the designated phantom's absorption (μ_a*) and reduced scattering (μ_s'*) coefficients to simulate the relevant attenuation profile (Table 1, Fig. 2). The maximum intensity of the profile decreased, when the μ_a* was enhanced as represented in each of the three subfigures (Fig. 2). On the other hand, the full width at half maximum (FWHM) was effected by the change of μ_a*.

The μ_s'* increasing from lowest to highest can be assessed, when

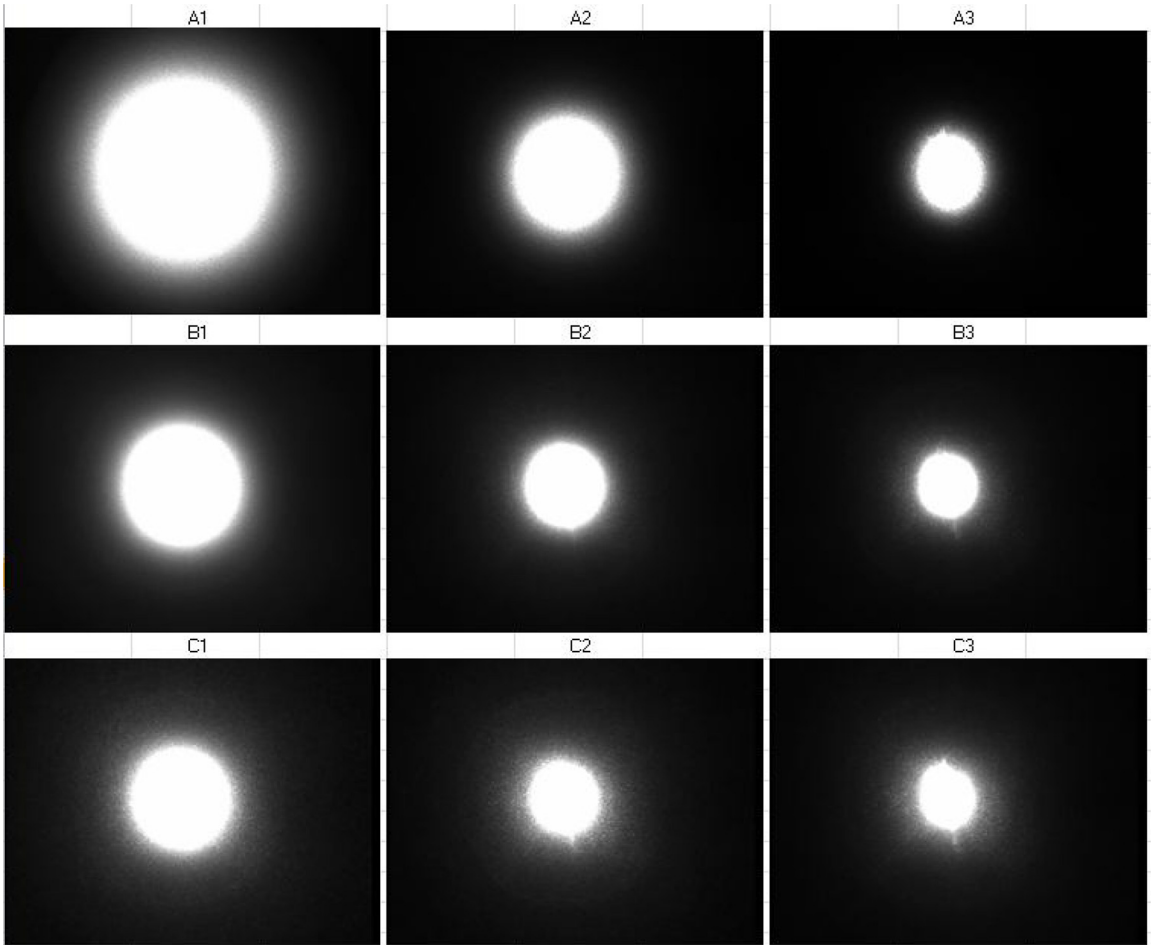

Fig. 1. Matrix of phantom images obtained by laser-light backscattering imaging (LLBI): matrix represents images in the order from lowest to highest values of absorption coefficient (1 to 3) and from lowest to highest reduced scattering coefficient (A to C).

comparing subfigures from left to right representing the set of phantoms A–C (Fig. 2). Here, an even more tremendous increase in the maximum intensity appeared; in the present set of phantoms by three magnitudes. The FWHM decreased, while the μ_s'* was enhanced. This is consistent with the literature, since on one hand it describes the effects of μ_a and μ_s' on the attenuation profiles as given in the text books providing a proof for the calculation routine. Furthermore, it provides an explanation for the encouraging calibration results found in fruit analysis, when using simple FWHM as published by many work groups.

The comparison of the three cases for analysing μ_a and μ_s' of each phantom in the present study is depicted in Fig. 3. For enhanced readability the reference values of the phantoms are shown again (Table 1, Fig. 3, upper). The ranges of set μ_a* and μ_s'* were similar to the value ranges found by the work group of Cubeddu (Cubeddu et al., 2001) and in the many cooperations with the group of Torricelli (Nicolai et al., 2007; Seifert et al., 2015) using time-resolved analysis. In the present study, the values appear distributed in the matrix as expected considering Table 1. In contrast, when using Farrell's model to

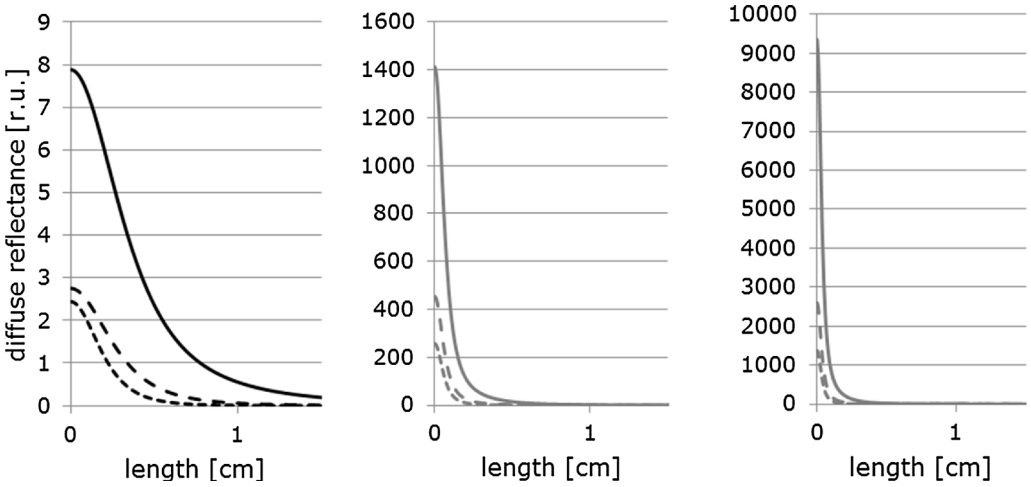

Fig. 2. Attenuation profiles of phantoms calculated by applying known coefficients of reduced scattering, μ_s'*, and absorption coefficient, μ_a* by means of Farrell's diffusion theory. Profiles are presented as diffuse reflectance at 940 nm, given in the order from lowest (__), medium (——), highest (….) absorption values for each phantom considering phantoms with lowest (set of 3 phantoms A, left), medium (set of phantoms B, middle), highest (set of phantoms C, right) reduced scattering coefficient.

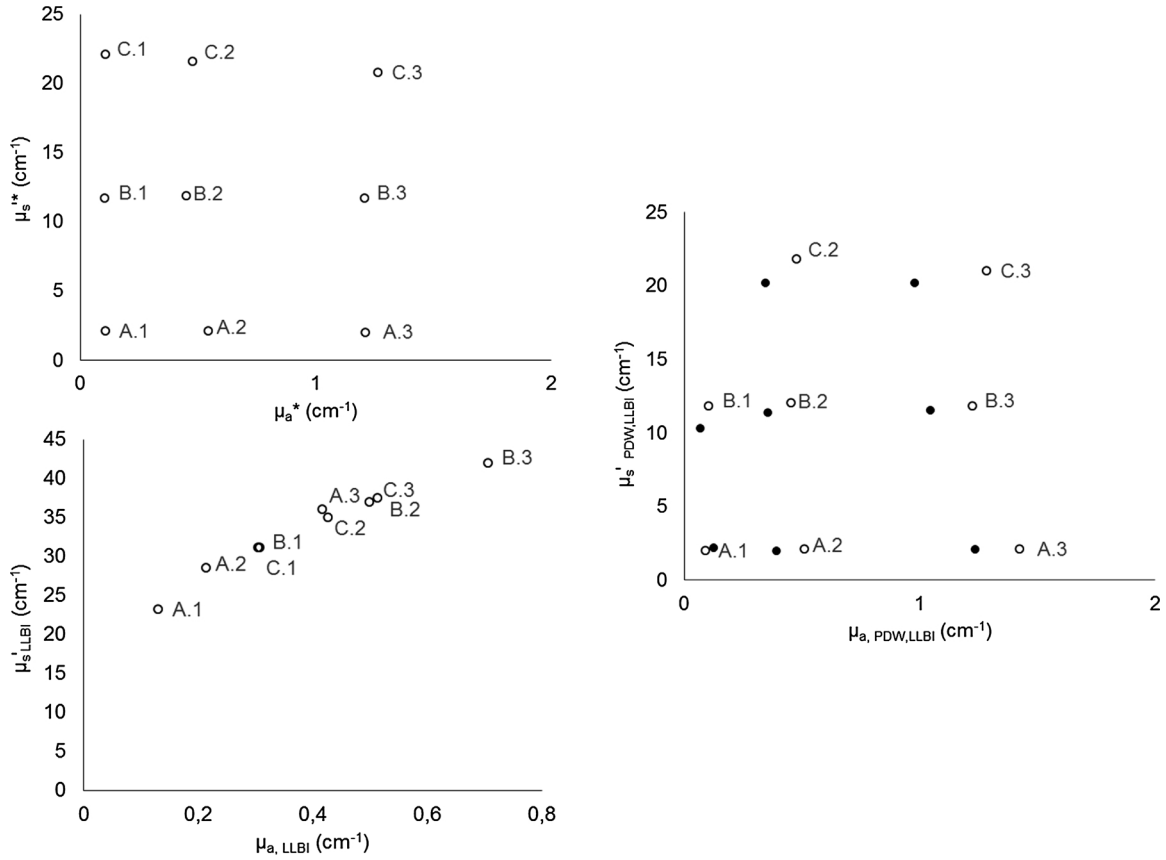

Fig. 3. The actual μ_a* and μ_s'* of phantoms (upper, from Table 1), mean values of $\mu_{a,LLBI}$ and $\mu_s'_{LLBI}$ estimated from radial attenuation profiles measured by LLBI (middle), estimated μ_s' (open symbols) when using μ_a* from destructive reference analysis and estimated μ_a (filled symbols) when using μ_s'* from reference analysis (lower).

calculate both, μ_a and μ_s', directly from the attenuation profiles measured by LLBI, the values appear on a saturation curve (Fig. 3, middle). Consequently, the fitting with Farrell's model had no capacity to distinguish the optical properties, when working on the sum attenuation profile. Since in this case, we had no measure available to transfer the data into the expected value range, the scale appears different in this figure. However, using μ_s'* from PDW spectroscopy and fitting only the μ_a from non-destructive LLBI readings and vice versa for μ_a* and μ_s', resulted in the separation of optical properties (Fig. 3, lower). Values appeared in the expected range. Enhanced divergence of the fitting result appeared in phantoms of high absorption (Fig. 3, lower). However, the rmse was reduced due to enhanced mean values. The overall rmse found for μ_a, when fixing μ_s'* was 16.68% and 2.79%, respectively. The rmse of μ_a and μ_s', when fixing μ_a* was 2.62% and 0.27%, respectively. Consequently, the results showed reduced measuring uncertainty, when setting the μ_a* fix and calculating μ_s'. This may be discouraging, since the non-destructive measurement of μ_a appears more valuable when calculating SSC, water content or pigment contents of fruit. However, even the roughly 20% measuring uncertainty may valuably improve the correct classification obtained in sorting lines.

Consequently, one optical property can be measured non-destructively, if the other one is known. However, it should be kept in mind that the anisotropy factor of phantoms was not subject to changes, since not the type or size of scatter but their number was varied.

Phantom C.1 was excluded in the LLBI analysis due to no result when fitting the optical properties by means of Farrell's model. This can be explained by the proportion of absorption and scattering coefficients of the phantom itself whereby phantom C.1 possess the lowest value of μ_a but the highest value of μ_s'.

Analysis using diffuseness level, which is defined by the ratio of μ'_s/μ_a, provides general overview in the potential to apply Farrell's diffusion theory. Doornboss and co-workers (Doornbos et al., 1999) suggested the ratio should be larger than a chosen limit, usually at least 10. Almost all phantoms showed a diffuseness level of $\mu_s'/\mu_a > 10$ except phantom A.2, A.3 and B.3. Hielscher et al. (1998) even suggested a stricter limit for diffuseness level with threshold value of more than 40. If 40 is set as lower limit for this analysis, B.1 and C.2 is pronounced as the most consistent one with diffuseness level of 113.1 and 45.3, respectively. Concluding, the experimental design using spatially resolved LLBI analysis coupled with Farrell's diffusion theory was sensible as long as one variable was taken from reference (here from PDW spectroscopy) for determining the other variable. The limit of diffusion theory for analysing attenuation profiles obtained with LLBI in the ranges of μ_a and μ_s' relevant for fruits was pointed out.

3.2. Analysing μ_a and μ_s' of pear

The μ_a* and μ_s'* from destructive PDW spectroscopy were compared with the proposed approach of using non-destructive LLBI measurements in combination with PDW spectroscopy. The μ_a* and μ_s'* values of the pears obtained from PDW spectroscopy and the μ_a and μ_s' values from LLBI developed similarly over time (Fig. 4). Results of ANOVA, however, indicated significant difference ($P > 0.05$) between μ_a* and μ_a values measured by PDW spectroscopy and LLBI. In contrast, μ_s' showed no significant difference, but a slight offset. The μ_a values changed inversely between first and second measurement, while no further changes were found considering following measuring days. The μ_s' values increased and remained constant in the following days, while μ_s'* decreased in the first days and remained constant in the following days.

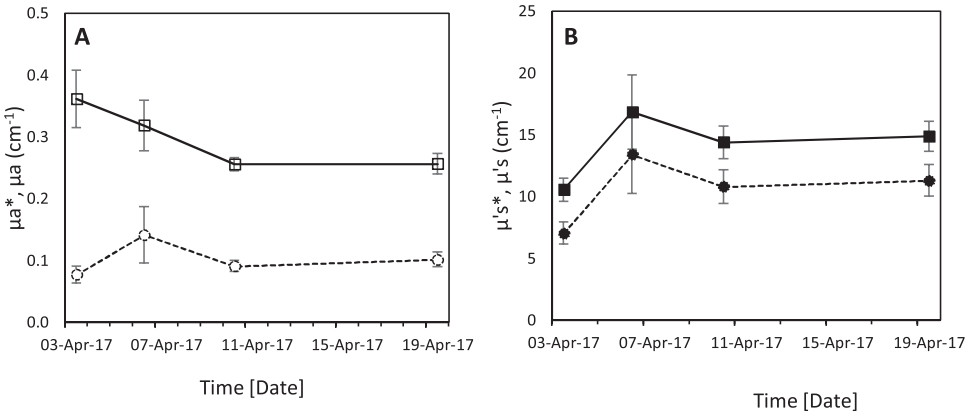

Fig. 4. Change of mean absorption coefficient, μ_a and μ_a* (A) and reduced scattering coefficient, μ_s' and μ_s'* (B) of pears by the date of measurement. The coefficients measured by PDW spectroscopy are represented by rectangles while the coefficients measured by LLBI are represented by circles. Error bars represent standard errors. PDW spectroscopy has been executed at 940 nm and LLBI at 1060 nm.

Some variance found may be due to the theory assuming that all injected photons will be represented in the attenuation profile. Even if the apparent attenuation of injected photons was reached within 2 cm, the dimension of pears with a mean diameter of 6.5 cm may have limited the measurement. The limited dimension of the pears also causes bias to the data obtained from PDW spectroscopy, since its theoretical background is based on photon interaction with infinite material. Even though the optical fibers were placed in the cortex of pear, the emitted photons may have interacted with structures of different optical properties, e.g., seeds, fruit skin. Qin and Lu (2008) reported that the error in measured optical properties by LLBI also could be due to the surface curvature of the samples. However, cosine correction of the LLBI data showed no error reduction in the phantoms (data not shown). Another variance in the values may appear due to the different wavelengths used in both methods, with 940 nm for PDW spectroscopy and 1060 nm in the LLBI analyses. The μ_s' spectrum of fruit is rather constant in the SWNIR, while the water absorption shows broad peaks in this range and particularly at 940 nm. The latter maybe the main influencing factor of the inverse results found when comparing measurements at 940 and 1060 nm, pointing to decreasing water content analysed by means of μ_a* at 940 nm.

Considering both approaches for measuring the optical properties, the μ_s'* and μ_s' values were always higher than μ_a* and μ_a, respectively. This is consistent with the earlier findings in which the scattering spectrum is generally more than 10 times enhanced in magnitude compared to the absorption spectrum due to the dominant scattering effect (Cubeddu et al., 2001). He et al. (2016) found that the μ_s' of pear in their study was more than 100 times of μ_a, hence later concluded that pear tissue is a high-albedo medium, still confirming that biological material is highly scattering (Fang et al., 2016).

For comparison, the μ_a* and μ_s'* derived from PDW spectroscopy were inserted in Farrell's model to simulate the relevant attenuation profiles (Fig. 5A), while LLBI attenuation profiles were directly measured in relative unit (Fig. 5B). The resulting shape of profiles appeared similar for both data sets, despite the appearance of flat beginning of measured LLBI attenuations profiles due to saturation of the camera chip. The signal decreased as the distance from the incident point increased. While the shape proofed reasonable, the attenuation profiles of the measuring days appeared with no consistent order. Day 1 of experiment exhibited the lowest values for PDW data. The attenuation profile measured on Day 1 with LLBI exhibited the lowest values only when removing the saturation area completely.

3.3. Prediction of pear quality

The pears developed as assumed considering its quality attributes. Water content of pears decreased ($P < 0.05$) from 85.07% to 82.45% over time in shelf life. A correlation of water content and μ_a* at 940 from PDW spectroscopy as well as μ_a obtained at 1060 nm in LLBI was found (Table 2). Frenkel and Hartman (2012) reported that the decline in water content in the fruit tissue during ripening either occurring naturally or induced by ethylene is strongly correlated with a decrease in swelling efficacy of cell wall. As water is lost from fruit cells, turgor pressure decreases, followed by cell shrinkage and consequently a reduction in fruit volume (Rhodes, 1980; Nagy et al., 2016; Nguyen et al., 2007). There appears to be a correlation between elastic modulus and ultimate strength of fruit tissue by which high turgor results in enhanced modulus of elasticity of the fruit (Chen and Thompson, 2000; Kojima et al., 2004). As pointed out by Schouten and co-workers, the major water loss appears in the beginning of shelf life, which is consistent with the present data of absorption as well as to a lower extend with scattering. Hashim et al. (2013) reported water content as the major influence to the behaviour of attenuation profile whereby difference ($P < 0.05$) was found between the control and treated samples as related to storage time in banana fruit.

A correlation of fruit flesh firmness and scattering properties has been assumed (McGlone et al., 1997; Qing et al., 2008; Qin et al., 2009; Mendoza et al., 2014). In the present study, the decrease of fruit flesh firmness from 93.8 N to 38.5 N was measured as expected. However, no parallel development of μ_s' and firmness has been found. This finding may be explained again by the change in water content, which in turn would reduce the elastic modulus. The water loss and its impact on cell turgor and refractive index may have even caused an increase of μ_s'. An interaction of firmness and elastic modulus, however, cannot be expected, since the elasticity depends highly from the water content, while the firmness appears less influenced by the water content, and consequently, the non-destructive analysis of firmness appears challenging (Zude et al., 2006).

An increase of SSC was found from 13.7% to 14.5%. The postharvest increase in SSC appears unusual for most fruit, but is well known in pears (Brandes and Zude-Sasse, 2019). It can be assumed that an increase in SSC results in enhanced values of μ_a measured at 940 or 1060 nm (Abe et al., 2000). The increased values of μ_a between first and second measuring day might be explained by the influence of enhanced SSC, while the water loss may have compromised this influence over the experimental period.

The R^2 of the attributes of fruit quality and μ_a and μ_s' (Table 2) appear consistently with the results obtained on the phantoms. Overall, both μ_a and μ_s' could be used to predict pears quality at enhanced R^2 values, when applying the LLBI analysis and reference data. This is likely expected since both properties relate to the physical and physicochemical properties of fruit, and each optical property provides different aspects of information. Interestingly, μ_s' provide quite strong prediction values for predicting water content, even if outperformed by the μ_a. This finding appears slightly below the range with the previous work (Adebayo et al., 2017), when using pears of higher fruit size and comparable to those found in other horticultural produce studied by Qin and Lu, (2008), whereby correlations were higher than 0.50 at all

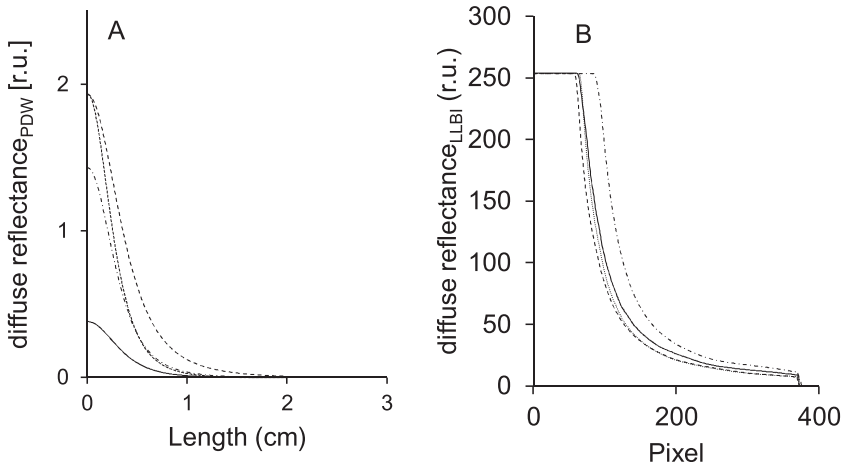

Fig. 5. Attenuation profiles of pears calculated by means of Farrell's diffusion theory using absorption and reduced scattering coefficients, μ_a* and μ_s'* from PDW spectroscopy at 940 nm (A) and raw intensities profiles obtained from LLBI images at 1060 nm (B) on Day 1 (__), Day 4 (._._), Day 8 (—) and Day 17 (……).

Table 2
Coefficient of determination of pear quality properties and (i) absorption coefficient (μ_a*) and reduced scattering coefficient (μ_s'*) analysed by destructive PDW spectroscopy; (ii) $\mu_{a,\ LLBI}$ or $\mu_s'_{LLBI}$, both analysed by laser-light backscattering imaging (LLBI) in one step; and (iii) referenced approach by LLBI considering μ_a with fix μ_s'* and μ_s' with fix μ_a'*.

Fruit attribute	μ_a*	$\mu_{a,LLBI}$	μ_a with fix $\mu s'$*	μ_s'*	$\mu_s'_{LLBI}$	μ_s' with fix μ_a*
Water content [%]	0.91	0.63	0.83	0.40	0.62	0.38
Firmness [N cm^{-2}]	0.07	0.78	0.52	0.07	0.01	0.06
SSC [%]	0.45	0.82	0.90	0.45	0.11	0.42

wavelengths between 500 and 1000 nm, with the maximum correlation coefficient of r = 0.66 at 790 nm.

4. Conclusion

Optical techniques are widely explored for sorting and grading agricultural produce and the feasibility of the techniques can be assumed. However, decoupling the optical properties which is important for a quantitative understanding of light interaction with fruit tissue is still of great challenge. Laser-light backscattering imaging and the analysis of the attenuation profile obtained by means of Farrell's diffusion theory showed no capacity to separate μ_a and μ_s', when measuring solid half-sphere phantoms having the same ranges of optical properties such as found in fruit. The analysis of one unknown variable was indeed confirmed, when one variable was fix according to reference data and should be investigated further. In fruit analysis, mainly the μ_a is of interest providing information on the chemical composition of the sample. Even the roughly 20% error found when calculating μ_a non-destructively may support the automated analysis of fruit.

Prediction of fruit quality by means of optical properties was hardly achieved in this study which may be explained by the fact that the physiological process behind the fruit quality is often accompanied with changes in chemical components and particularly the water content, which appeared correlated with both μ_a and μ_s'. It may be concluded that the parallel progress of different quality attributes makes it hardly possible to judge the prediction capacity of optical properties. This also means that, if reliable data on the optical properties are available, the prediction of more specific fruit attributes (such as the water or pigment content) may become a more robust tool.

Contributions

Manuela Zude-Sasse developed the idea and layout of the present study. Together with Christian Regen, she did the data analysis of LLBI, and with Shila Hashim, she wrote the mansucript. Shila Hashim conducted the experiments and did the statistical analysis. Roland Hass contributed to the experimental planning for the pear measurements by PDW spectroscopy, supervised them, and worked on the construction of the optical fiber array used for these measurements. Nabarun Polley supported Shila Hashim in the experimental execution of the characterization of the pears by PDW spectroscopy and worked on the related data analysis. Christian Regen programmed the data analysis of LLBI and carried out the LLBI measurements.

Acknowledgements

The authors are grateful for the financial support from Universiti Putra Malaysia. The work on the PDW spectroscopy part was supported by the German Federal Ministry of Education and Research (BMBF, grant 03Z22AN12).

References

Abe, H., Iyo, C., Kawano, S., 2000. A study on the universality of a calibration with sample temperature compensation. J. Near Infrared Spectrosc. 8, 209–213.
Adebayo, S.E., Hashim, N., Abdan, K., Hanafi, M., Regen, C., Hass, R., Zude-Sasse, M., 2017. Using absorption and reduced scattering coefficients for non-destructive analyses of fruit flesh firmness and soluble solids content in pear (*Pyrus communis*' Conference') - an update when using diffusion theory. Postharvest Biol. Technol. 130, 56–63.
Baranyai, L., Zude, M., 2009. Analysis of laser light propagation in kiwifruit using backscattering imaging and Monte Carlo simulation. Comput. Electron. Agric. 69, 33–39.
Birth, G.S., 1976. How light interacts with foods. In: Gaffney JrJ.J. (Ed.), Quality Detection in Foods. American Society for Agricultural Engineering, St. Joseph, MI, pp. 6–11.
Brandes, N., Zude-Sasse, M., 2019. HeliyonRespiratory Pattern in' Conference' Pear Throughout Fruit Development52019. Respiratory Pattern in' Conference' Pear Throughout Fruit Development 5, e01160.
Bressel, L., Hass, R., Reich, O., 2013. Particle sizing in highly turbid dispersions by photon density wave spectroscopy. J. Quant. Spectrosc. Radiat. Trans. 126, 122–129.
Cao, F., Wu, D., He, Y., 2010. Soluble solids content and pH prediction and varieties discrimination of grapes based on visible-near infrared spectroscopy. Comput. Electron. Agric. 71, S15–S18.
Chen, P., 1978. Use of optical properties of food materials in quality evaluation and materials sorting. J. Food Process Eng. 2 (4), 307–322.
Chen, P., Thompson, J., 2000. Development of a Firmness Tester for Pears. The California Pears Advisory Board, Post Harvest Research Report 2000.
Cubeddu, R., D'Andrea, C., Pifferi, A., Taroni, P., Torricelli, A., Valentini, G., Ruiz-Altisent, M., Valero, C., Ortiz, C., Dover, C., Johnson, D., 2001. Time-resolved reflectance spectroscopy applied to the nondestructive monitoring of the internal optical properties in apples. Appl. Spectrosc. 55 (10), 1368–1374.
Doornbos, R.M.P., Aalders, M.C., Cross, F.W., Sterenborg, H., 1999. The determination of in vivo human tissue optical properties and absolute chromophore concentrations using spatially resolved steady-state diffuse reflectance spectroscopy. Phys. Med. Biol. 44, 967–981.

Fang, Z.-H., Fu, X.-P., He, X.-M., 2016. Investigation of absorption and scattering characteristics of kiwifruit tissue using a single integrating sphere system. J. Zhejiang Univ.-Sci. B (Biomed. Biotechnol.) 17 (6), 484–492.
Farrell, T.J., Patterson, M.S., 1992. A diffusion theory model of spatially resolved, steady-state diffuse reflectance for the noninvasive determination of tissue optical properties in vivo. Med. Phys. 19 (4), 879–888.
Frenkel, C., Hartman, T.G., 2012. Decrease in fruit moisture content heralds and might launch the onset of ripening processes. J. Food Sci. 77 (10), S365–S376.
Groenhuis, R.A.J., Ferwerda, H.A., Bosch, J.J.T., 1983a. Scattering and absorption of turbid materials determined from reflection measurements. 1: theory. App. Opt. 22, 2456–2462.
Groenhuis, R.A.J., Ferwerda, H.A., Bosch, J.J.T., 1983b. Scattering and absorption of turbid materials determined from reflection measurements. 1: Measuring method and calibration. App. Opt. 22, 2463–2467.
Hashim, N., Pflanz, M., Regen, C., Janius, R.B., Abdul Rahman, R., Osman, A., Shitan, M., Zude, M., 2013. An approach for monitoring the chilling injury appearance in bananas by means of backscattering imaging. J. Food Eng. 116, 28–36.
Hass, R., Munzke, D., Ruiz, S.V., Tippmann, J., Reich, O., 2015. Optical monitoring of chemical processes in turbid biogenic liquid dispersions by Photon Density Wave spectroscopy. Anal. Bioanal. Chem. 407, 2791–2802.
He, X., Fu, X., Rao, X., Fang, Z., 2016. Assessing firmness and SSC of pears based on absorption and scattering properties using an automatic integrating sphere system from 400 to 1150nm. Postharvest Biol. Technol. 121, 62–70.
Hielscher, A.H., Alcouffe, R.E., Barbour, R.L., 1998. Comparison of finite-difference transport and diffusion calculations for photon migration in homogeneous and heterogeneous tissues. Phys. Med. Biol. 43 (5), 1285–1302.
Kojima, T., Fujita, S., Tanaka, M., 2004. Plant compounds and fruit texture: the case of pear. Texture in Food: Volume 2: Solids Foods. pp. 259–263.
Lorente, D., Zude, M., Idler, C., Gómez-Sanchis, J., Blasco, J., 2015. Laser-light backscattering imaging for early decay detection in citrus fruit using both a statistical and a physical model. J. Food Eng. 154, 76–85.
Lu, Y., Lu, R., 2018. Structured-illumination reflectance imaging coupled with phase analysis techniques for surface profiling of apples. J. Food Eng. 232, 11–20.
McGlone, V.A., Abe, H., Kawano, S., 1997. Kiwifruit firmness by near-infrared light scattering. J. Near Infrared Spectrosc. 5, 83–89.
Mendoza, F., Lu, R., Cen, H., 2014. Grading of apples based on firmness and soluble solids content using Vis/SWNIR spectroscopy and spectral scattering techniques. J. Food Eng. 125, 59–68.
Nagy, A., Riczu, P., Tamás, J., 2016. Spectral evaluation of apple fruit ripening and pigment content alteration. Sci. Hortic. 201, 256–264.
Nguyen, T.A., Verboven, P., Schenk, A., Nicolai, B.M., 2007. Prediction of water loss from pears (*Pyrus communis* cv. conference) during controlled atmosphere storage as affected by relative humidity. J. Food Eng. 83, 149–155.
Nicolai, B.M., Beullens, K., Bobelyn, E., Peirs, A., Saeys, W., Theron, K.I., Lammertyn, J., 2007. Nondestructive measurement of fruit and vegetable quality by means of NIR spectroscopy: a review. Postharvest Biol. Technol. 46, 99–118.
Nicolaï, B.M., Verlinden, B.E., Desmet, M., Saevels, S., Saeys, W., Theron, K., Cubeddu, R., Pifferi, A., Torricelli, A., 2008. Time-resolved and continuous wave NIR reflectance spectroscopy to predict soluble solids content and firmness of pear. Postharvest Biol. Technol. 47 (1), 68–74.
Prahl, S.A., van Gemert, M.J., Welch, A.J., 1993. Determining the optical properties of turbid media by using the adding–doubling method. Appl. Opt. 32, 559–568.
Qin, J., Lu, R., 2008. Measurement of the optical properties of fruits and vegetables using spatially resolved hyperspectral diffuse reflectance imaging technique. Postharvest Biol. Technol. 49 (3), 355–365.
Qin, J., Lu, R., Peng, Y., 2009. Prediction of apple internal quality using spectral absorption and scattering properties. Trans. ASABE 52, 499–507.
Qing, Z.S., Ji, B.P., Zude, M., 2008. Non-destructive analyses of apple quality parameters by means of laser-induced light backscattering imaging. Postharvest Biol. Technol. 48, 215–222.
Reich, O., Lohmannsroben, H., Schael, F., 2003. Optical sensing with photon density waves: investigation of model media. Phys. Chem. Chem. Phys. 5, 5182–5187.
Rhodes, M.J.C., 1980. The maturation and ripening of fruits. In: Thimann, K.V. (Ed.), Senescene in Plants. CRC Press, Inc., Boca Roton, F.L, pp. 157–205.
Rowe, P.I., Künnemeyer, R., McGlone, A., Talele, S., Martinsen, P., Seelye, R., 2014. Relationship between tissue firmness and optical properties of 'Royal Gala' apples from 400 to 1050 nm. Postharvest Biol. Technol. 94, 89–96.
Schmitt, J.M., Zhou, G.X., Walker, E.C., Wall, R.T., 1990. Multilayer model of photon diffusion in skin. J. Opt. Soc. Am. A 7, 2141–2153.
Seifert, B., Zude, M., Spinelli, L., Torricelli, A., 2015. Optical properties of developing pip and stone fruit reveal underlying structural changes. Physiol. Plant. 153, 327–336. https://doi.org/10.1111/ppl.12232.
Steinke, J.M., Shepherd, A.P., 1986. Diffuse reflectance of whole blood: model for a diverging light beam. IEEE Trans. Biomed. Eng. 34, 826–833.
Sun, J., Künnemeyer, R., McGlone, A., Rowe, P., 2016. Multispectral scattering imaging and NIR interactance for apple firmness predictions. Postharvest Biol. Technol. 119, 58–68.
Vargas Ruiz, S., Hass, R., Reich, O., 2012. Optical monitoring of milk fat phase transition within homogenized fresh milk by photon density wave spectroscopy. Int. Dairy J. 26, 120–126.
Zude, M., Herold, B., Roger, J.M., Landahl, S., Bellon-Maurel, V., 2006. Non-destructive tests on the prediction of apple fruit properties at the tree and in shelf life. J. Food Eng. 77, 254–260.
Zude, M., Pflanz, M., Dosche, K., Spinelli, L., Torricelli, A., 2011. Non-destructive analysis of anthocyanins in cherries by means of Lambert-Beer and multivariate regression based on spectroscopy and scatter correction using time-resolved analysis. J. Food Eng. 103, 68–75.